

FORMATION OF CUSPATE FORELAND BEHIND AN ISLAND UNDER WAVES INCIDENT FROM TWO OPPOSING DIRECTIONS

Akio Kobayashi¹, Takaaki Uda², Takuya Yokota¹, Yasuhito Noshi¹ and Kazuma Nishimura¹

Long-term shoreline changes of a cusped foreland behind Okinoshima Island located in Tateyama Bay were investigated, and a beach survey was carried out using an RTK-GPS on May 2, 2018. Then, numerical simulation of the formation and deformation of a cusped foreland between 1941 and 2012 was carried out using the BG model (a model for predicting 3-D beach changes based on Bagnold's concept). It was found that sand, which was deposited on the shallow sea associated with the increase in ground level during the Kanto Great Earthquake that occurred in 1923, accumulated to form a cusped foreland.

Keywords: land-tied island; cusped foreland; increase in ground level; BG model; beach changes; Okinoshima Island; numerical simulation

INTRODUCTION

A land-tied island can be formed owing to the seaward (landward) extension of a cusped foreland from the mainland (an offshore island). The primary cause is the diffraction of waves incident from the direction dividing the island into two or the action of waves incident from opposing directions on both sides of the island. Regarding the extension of the cusped foreland to form a land-tied island under waves incident from two opposing directions, Miyahara et al. (2014) investigated the formation mechanism using the BG model (a model for predicting 3-D beach changes based on Bagnold's concept), taking the land-tied island on Shodoshima Island in the Seto Inland Sea as an example. However, the formation process of the cusped foreland behind an island has not been sufficiently studied. In particular, the difference in the shape of the cusped foreland when waves are incident from the direction dividing the island into two and from two opposing directions has not been fully investigated. Okinoshima Island located in Tateyama Bay in Japan is a typical land-tied island. In Tateyama Bay, where Okinoshima Island is located, the ground level increased approximately 1.6 m immediately after the Kanto Great Earthquake in 1923, and a shallow sea was formed around the island (Chiba Prefectural Government, 1996). As a result, wave action on the sand particles increased, and sand was collected behind the island owing to the wave action with a rapid decrease in water depth, although sand deposited in the sea surrounding the island was difficult to move by waves before the ground uplift because of the large water depth. However, no accurate explanation for the sand accumulation has been given. Furuya et al. (2014) investigated the shoreline changes around the island using aerial photographs together with field observation. In this study, long-term changes in the shoreline on this island were investigated, and numerical simulation of the formation and deformation of the cusped foreland between 1941 and 2012 was carried out using the BG model (Uda et al., 2018).

CUSPATE FORELAND FORMED BEHIND OKINOSHIMA ISLAND AND ITS DEFORMATION

Okinoshima Island is located 6.3 km east of Sunosaki Point and 5.3 km south of Ofusa Point in Tateyama Bay on Boso Peninsula, as shown in **Fig. 1(a)**. **Figure 1(b)** shows an enlarged satellite image of the rectangular area shown in **Fig. 1(a)**. Since Okinoshima Island is bounded by Boso Peninsula on the south side, direct action of rough waves from the Pacific Ocean to the coast is rare, and wind waves generated in Tateyama Bay are mainly incident to the coast. The land-tied island is located in front of the seawall along the base of the Japan Maritime Self-Defense Force.

Figure 2 shows a wind rose for the ten-year period between 2007 and 2017 measured at AMEDAS Tateyama together with the direction of the seawall along the base. The most frequent wind direction is 16% for SW, followed by N and NNE (9% and 7%, respectively). In each case, wind blows from a direction that makes a small angle relative to the direction of the seawall, and the probability of the occurrence of WNW wind, which blows from the direction normal to the seawall, is only 5%. From these facts, it is assumed that the cusped foreland behind this island was not formed by waves that propagate from the direction of the centerline of the island but was formed by two waves propagating in opposing directions on the northeast and southwest sides of the island.

¹ Department of Oceanic Architecture and Engineering, College of Science and Technology, Nihon University, 7-24-1 Narashinodai, Funabashi, Chiba 274-8501, Japan

² Public Works Research Center, 1-6-4 Taito, Taito, Tokyo 110-0016, Japan

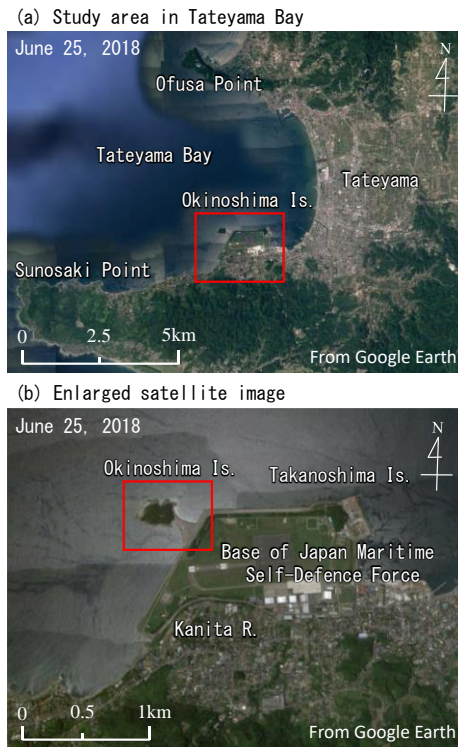


Figure 1. Location of Okinoshima Island in Tateyama Bay.

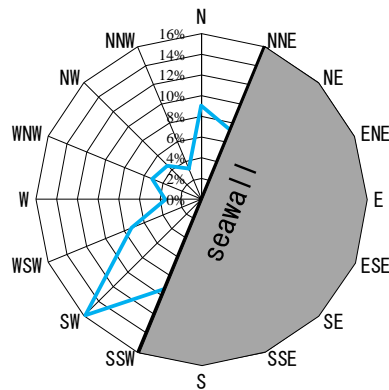


Figure 2. Wind rose at AMEDAS Tateyama.

Figure 3 shows the nautical chart produced in 1941 after the uplift of the ground owing to the Kanto Great Earthquake that occurred in 1923. A shallow seabed of 1–2 m depth extended around the island. The changes in the cusped foreland behind the island between 1947 and 2012 are shown in Figure 4 together with the tide levels when the aerial photographs were taken. In 1947, no cusped foreland had formed behind the island. A long, slender cusped foreland extended from the southeast end of the island to the seawall along the base of the Japan Maritime Self-Defence Force until 1963. Then, until 1975, the width of the sandbar increased at a location where the cusped foreland meets the seawall.

From 1975 to 1990, the width of the cusped foreland behind the island increased. In particular, the amount of sand deposited in front of the seawall in the south part markedly increased. By 2012, the shoreline had significantly advanced on the south side, although the shoreline changes on the north side of the cusped foreland were small, resulting in the increase in the sandbar width on the south side of the cusped foreland.

Regarding the formation of this cusped foreland, Furuya et al. (2014) considered that the sand necessary for the formation of this cusped foreland was mainly supplied from the Kanita River located south of this island, and the supplied sand was transported by northward longshore sand transport. Furthermore, they showed that part of sand was transported across the sandbar as the sand blown by the

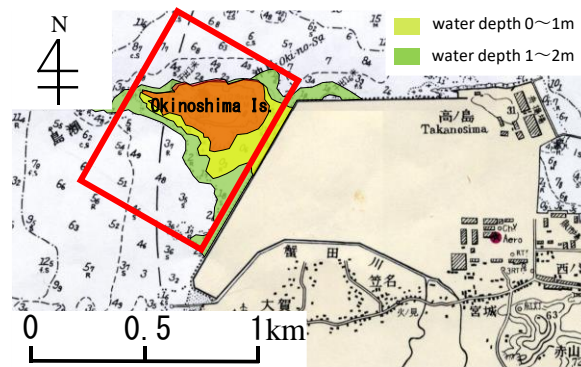


Figure 3. Nautical chart produced in 1941.

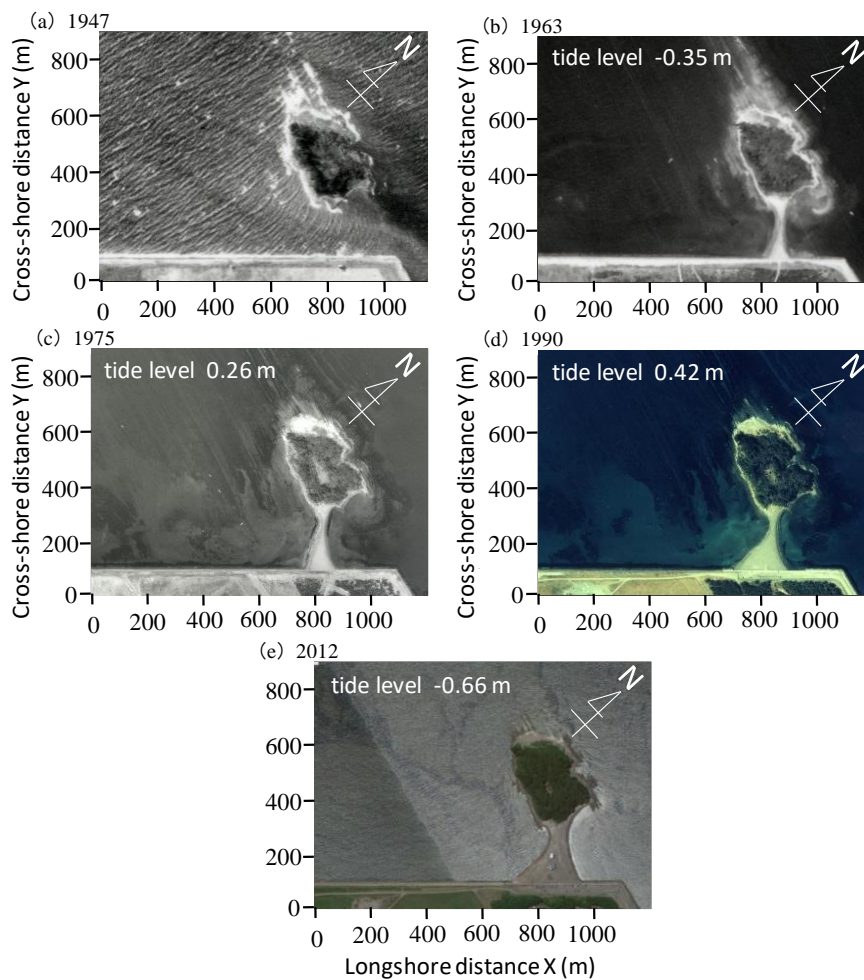


Figure 4. Changes in cuspate foreland behind Okinoshima Island between 1947 and 2012.

west wind, which prevails in winter in this area. However, the seawall was exposed to waves in a 700 m stretch south of the island, as shown in Fig. 1, and no sand to be transported by longshore sand transport is deposited in this area. Also, the mouth of the Kanita River faces southwest, which is the direction opposite to the expected. Thus, it is difficult to assume that the sand composing the sandbar of the island has been transported from a nearby source around the island by sand transport owing to waves. In this study, we hypothesized that sand movement owing to waves was initiated by the ground uplift, and sand accumulated on the lee of the island. To investigate this hypothesis, topographic changes of the sandbar were investigated using past aerial photographs, and a topographic survey around the sandbar was carried out on May 2, 2018 using an RTK-GPS. Then, the development of the

sandbar behind the island in the period of 71 years between 1941 and 2012 was reproduced using the BG model.

RESULTS OF FIELD OBSERVATION OF SANDBAR AND CROSS-SHORE PROFILES

Figure 5 shows a satellite image of Okinoshima Island and the cusped foreland behind the island, taken on January 17, 2017. The arrangement of survey lines and the locations where site photographs were taken are also shown in the figure. Twelve transects were set parallel to the seawall at 20 m intervals to cover the entire sandbar. Site photographs were taken at stations A–E on November 23, 2018. The island is 240 m wide and 250 m long. The shoreline has an arch on the north side, whereas a hooked shoreline has formed on the south side of the island.

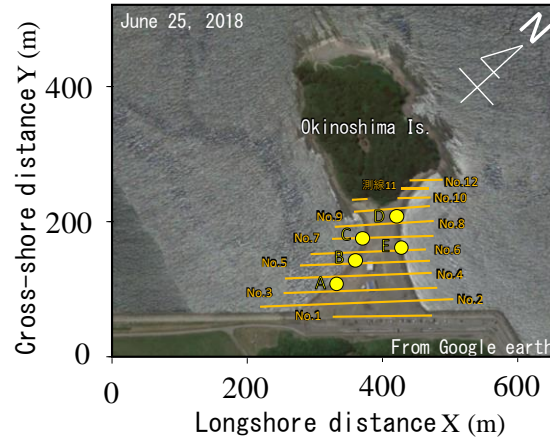


Figure 5. Arrangement of twelve transects crossing sandbar.



Figure 6. Shoreline obliquely intersected with seawall and a high berm (St. A).



Figure 7. Foreshore slope of 1/10 (St. B).

On the south side of the cusped foreland, the shoreline has obliquely intersects with the seawall, and a high berm has formed at St. A near the south end of the shoreline, as shown in **Fig. 6**. When approaching the island along the shoreline of the cusped foreland, the berm formation ceases, and a uniform beach of 1/10 slope has formed at St. B (**Fig. 7**). **Figure 8** shows the shoreline condition at St. C on the lee of the island, where a beach with a gentle slope extends without berm formation. Thus, the berm formation on the south side of the cusped foreland is in strong contrast to the uniform slope on the lee of the island, implying that the wave height markedly decreased from the front of the seawall to the lee of the island.

Figure 9 shows the beach at St. D on the northeast side of the cusped foreland, facing the rock of the island located at the west end. Different from the condition on the south side of the cusped foreland, debris has been deposited continuously along the high tide shoreline, and a scarp has formed near the high tide shoreline. A concave shoreline also extends on the east side of the beach with scarp formation and the deposition of debris near the high tide shoreline, as shown in **Fig. 10**. **Figure 11** shows a



Figure 8. Shoreline condition on lee of island (St. C).



Figure 9. North beach on northeast side of cusped foreland (St. D)



Figure 10. Concave shoreline, scarp formation and deposition of debris on east side of the beach (St. D).

photograph taken during the measurement of the foreshore slope of 1/10 at St. E in the middle of the foreshore on the northeast side of the cusped foreland. The formation of a scarp and the deposition of debris near the high tide shoreline on the north side of the cusped foreland are in strong contrast to the formation of a berm on the south side, which indicates the depositional feature of the beach. Thus, it is assumed that the beaches on both sides of the cusped foreland have an independent sand transport system, except for the sand transport by wind.

Figure 12 shows longitudinal profiles along four of the transects shown in **Fig. 5**. The beach has a flat surface along every transect, and the beach width decreases from transect No. 2, close to the seawall, to transect No. 8 behind the island with decreasing height of the beach surface. From these



Figure 11. Foreshore slope of 1/10 on northeast side of the cusped foreland (St. E).

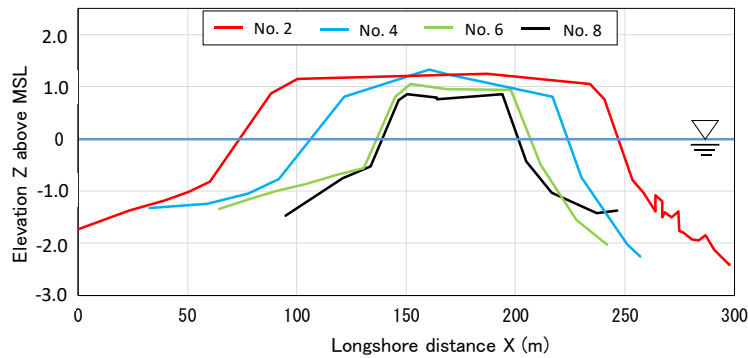


Figure 12. Longitudinal profiles across four transects.

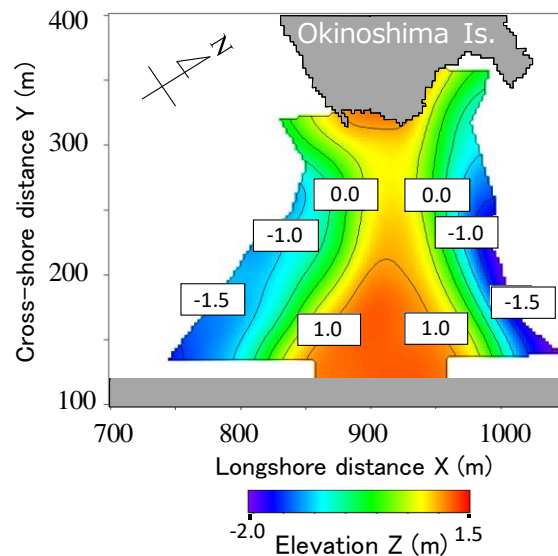


Figure 13. Measured topography of the cusped foreland.

facts, it is found that the wave height decreases on the lee of the island owing to the wave-sheltering effect, even though waves are incident from two opposing directions. **Figure 12** shows that the berm heights on the south and north beaches are 0.97 and 0.91 m, respectively, on average, i.e., the berm heights on both sides of the cusped foreland were almost equivalent.

Figure 13 shows the measured topography of the cusped foreland. Comparison of the beach widths immediately behind the island and far from the lee of the island in the typical form of a cusped foreland shows that the beach width far from the island is much greater than that on the lee of the island. However, the difference in beach width is small at the cusped foreland behind this island, implying that the cusped foreland was not formed by unidirectional waves but was formed by waves incident from two opposing directions.

PREDICTION OF FORMATION OF CUSPATE FORELAND USING BG MODEL

On the basis of the meteorological data collected between 2007 and 2012 at AMEDAS Tateyama observatory, wave characteristics were calculated by the SMB method, from the fetch distance and wind direction when the wind velocity reached the daily maximum value. First, the daily significant wave height $H_{1/3}$ and wave period $T_{1/3}$ were calculated, and the energy mean wave height was obtained. A single wave was assumed for waves incident from the directions of N and NNE, and a single wave with the energy mean wave height was assumed to be incident from $N11.25^\circ E$, the mean direction between N and NNE. For the wave period, the overall average of the period was employed. Finally, the energy mean wave height became 0.28 m with a period of 2.0 s for waves incident from $N11.25^\circ E$. Similarly, the energy mean wave height for waves incident from the direction of SW became 0.27 m with a period of 1.9 s.

The probabilities of occurrence of northerly waves are 9.0% and 7.3% for the directions of N and NNE, respectively, and the sum is 16.3%, whereas the probability of occurrence from the direction of

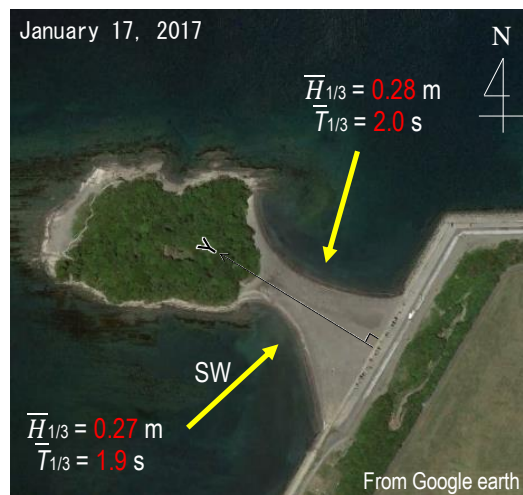


Figure 14. Energy mean waves around the island.

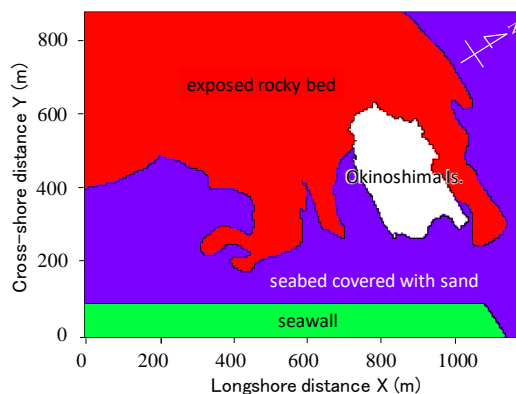


Figure 15. Initial topography and distribution of exposed rocky bed.

SW is 15.8%, i.e., waves with approximately the same probability of occurrence are incident from the opposing directions. **Figure 14** shows the calculation results of $\bar{H}_{1/3}$ and $\bar{T}_{1/3}$ in each direction. The waves incident from the two opposing directions make an angle of $\pm 74^\circ$ relative to the direction (Y -axis) normal to the seawall, as shown in **Fig. 14**.

The calculation domain is a rectangular area of 1.2 km length and 0.87 km width in the X - and Y -directions, respectively. Two calculations were carried out; in Case 1, waves were assumed to be incident from two directions, namely, SW and N+11.25°E. Waves with a significant wave height of 0.3 m, which is a rounded value of the calculated wave height, were incident from the direction, which makes an angle of $\pm 74^\circ$ relative to the Y -axis. In Case 2, waves were assumed to be incident from the direction of WNW to compare the change in shape of the cusped foreland relative to Case 1, although the wave incidence from this direction was rare, as seen in **Fig. 2**; the probability of occurrence of wind from this direction was as low as 5%. The wave direction in Case 2 was set to 0° with the same wave height of 0.3 m.

From the aerial photographs shown in **Fig. 4**, the exposed rocky bed and sandy bed can be clearly separated in the shallow sea around the island in the aerial photograph taken in 1975. **Figure 15** shows the distributions of the rocky and sandy beds. The exposed rocky bed distributes and approaches the island in complicated forms, and the nearby area of the exposed rocky bed is covered with sand. In this study, the exposed rocky bed was assumed to be a fixed bed. The berm height h_R was set to 1.0 m on the basis of the measured longitudinal profiles, as shown in **Fig. 12**. Since the depth of closure h_c is given by (2-3) h_R (Uda, 1997), we set it to 2 m in this study. The equilibrium slope was set 1/10 from the measured values, as shown in **Figs. 7** and **11**. **Table 1** shows the calculation conditions.

Figure 16 shows the planar distribution of the K_d value around the island determined by the directional spreading method for irregular waves. In Case 1, waves incident from two opposing directions are diffracted around the island and meet behind the island. In Case 2, diffraction of a single wave occurs at the offshore end of the island and the rock located at the north end of the island.

When waves of the same height are incident from two opposing directions as in Case 1 and they meet behind the island, the action of waves from both directions will approximately counteract each

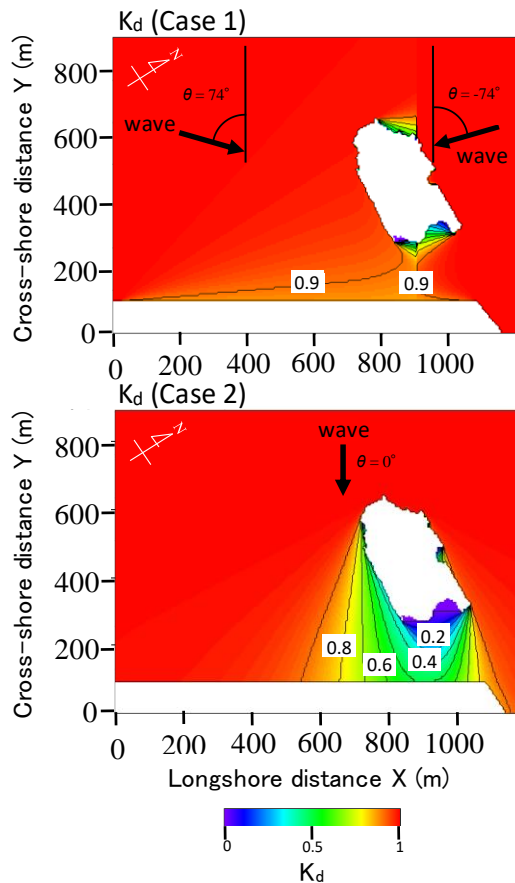


Figure 16. Distribution of K_d value around the island calculated by directional spreading method.

other near the centerline of the island. As a result, the energy fluxes of the waves with two opposing directions on both sides of the island are assumed to balance each other, resulting in zero net sand transport. Thus, we assumed an impermeable wall along the meeting line of waves behind the island in Case 2.

Table 1. Calculation conditions.		
Incident wave conditions	Case 1: $H=0.3$ m, Case 2: $H=0.3$ m	
Wave period	Case 1: $T=2.0$ s, Case 2: $T=2.0$ s	
Wave direction	Case 1: $\theta = 74^\circ$, $\theta = -74^\circ$	
	Case 2: $\theta = 0^\circ$	
Tide condition	MSL 0.0 m	
Berm height h_R (m), Depth of closure h_c (m)	$h_R=1.0$ m, $h_c=2.0$ m	
Equilibrium slope $\tan\beta_c$	1/10	
Coefficient of longshore sand transport	Coefficient of longshore sand transport	$K_s=1.0 \times 10^{-1}$
	Ozasa and Brampton's Coefficient	$K_2=1.62K_s$
	Coefficient of cross-shore sand transport	$K_r=0.2K_s$
Depth distribution of sand transport	uniform	
Calculation meshes	$\Delta X=\Delta Y=5.0$ m	
Time step	$\Delta t=0.05$ hr	
Duration of calculation	1941-2012	

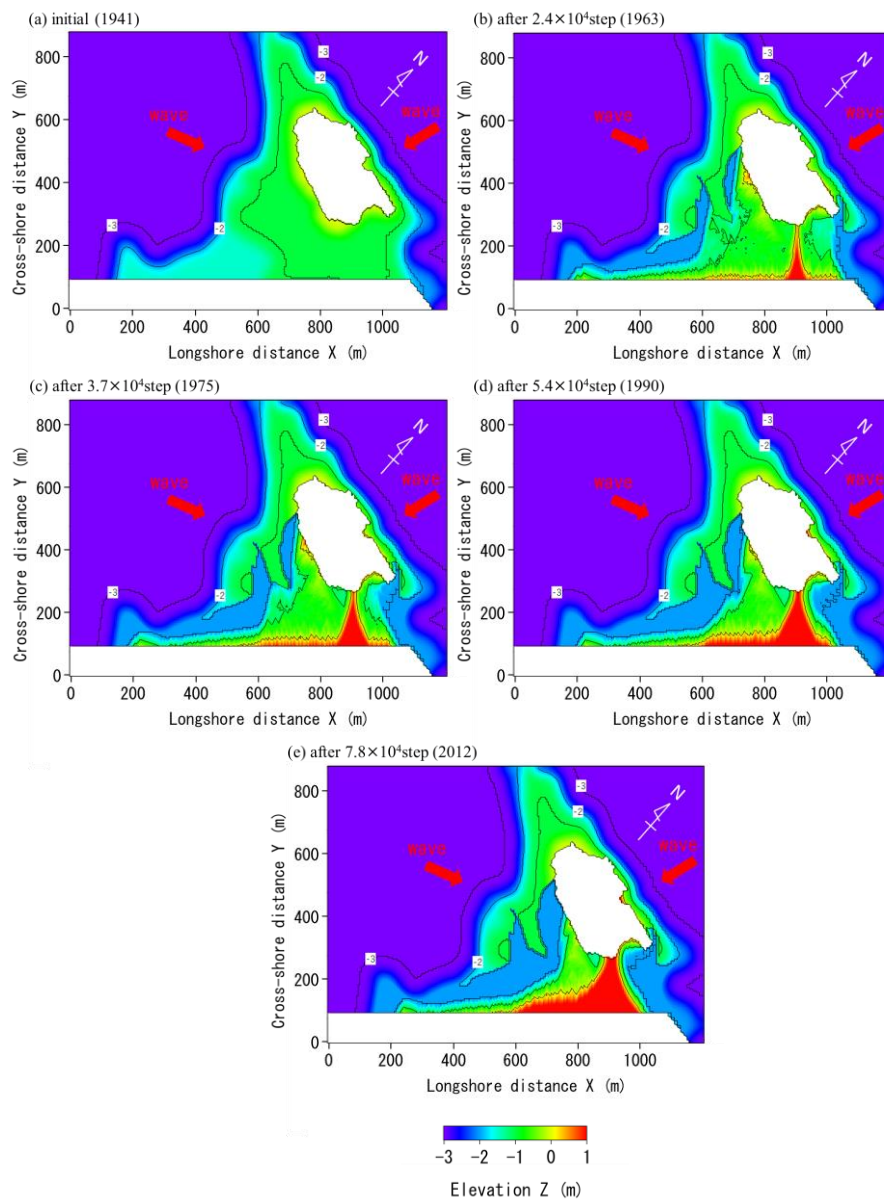


Figure 17. Formation of cusped foreland behind island (Case 1).

The duration of the calculation was set as follows. As shown in **Fig. 4**, there was no sandbar in 1947, but there was a slender sandbar in 1963. By setting 1941 as the initial year, the time steps to reproduce the topography in 1963 were obtained, given waves with a constant height, and with reference to this duration, the time steps corresponding to the real time were determined.

Figure 17 shows the calculation results in Case 1. As a result of the calculation, sand deposited on the seabed between 1 m depth and the island in the calculation domain was transported behind the island owing to waves incident from two opposing directions, and a slender sandbar was formed. Until 1963, it was connected to the island. Then, the sandbar continued to develop over time, and the beach width at the location where the sandbar connected to the seawall increased. Furthermore, the beach width increased until 2012. The results of the formation of a slender sandbar and the southward expansion of sandbar are in good agreement with the measurement results. During the development of the sandbar, the wave angle relative to the direction normal to the seawall was as large as 74° in the area along the seawall; thus, the topographic changes associated with high-angle wave instability (Ashton et al., 2001) occurred. However, it disappeared over time.

Figure 18 shows the results of Case 2. Although sand was deposited in front of the seawall behind the island and its size gradually increased over time, a tombolo connecting to the island was not formed within the calculation time. **Figure 19** shows the predicted results of the cusped foreland in Cases 1

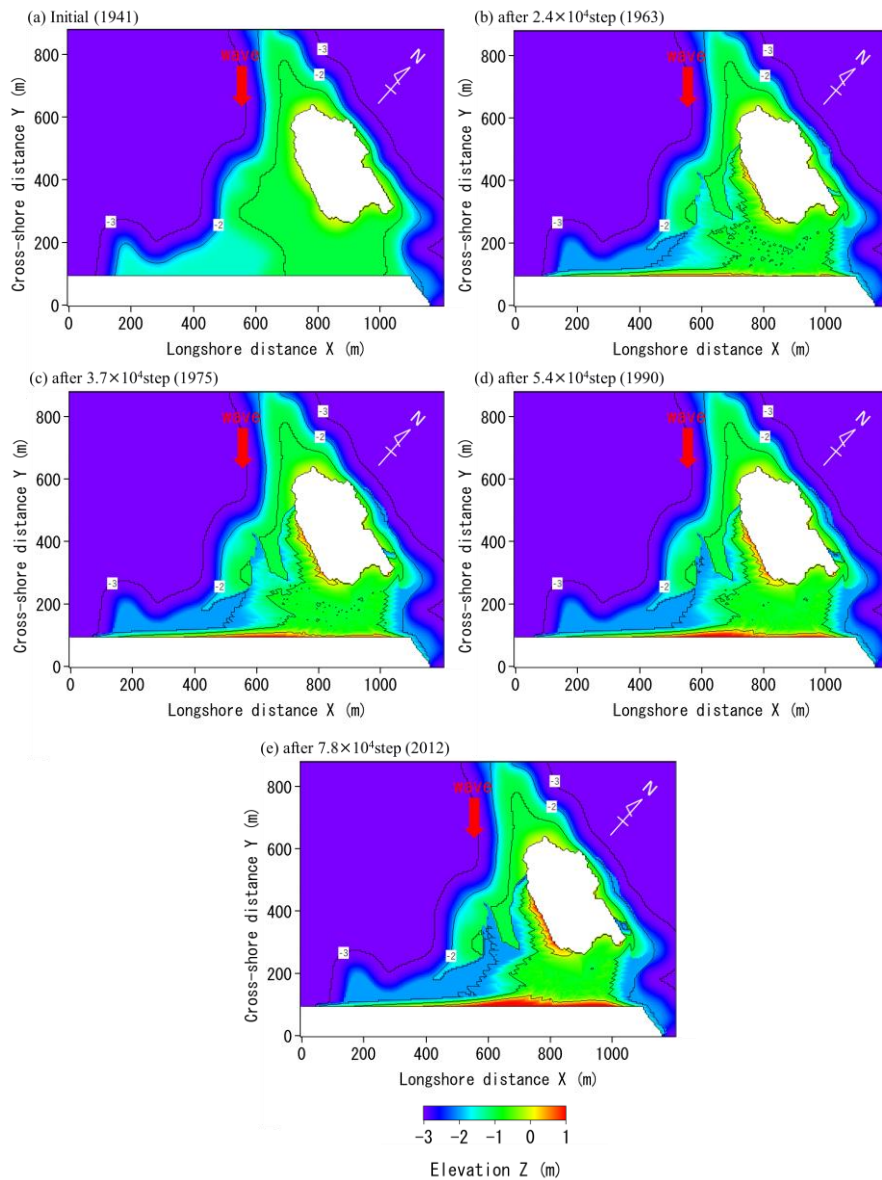


Figure 18. Formation of cusped foreland behind island (Case 2).

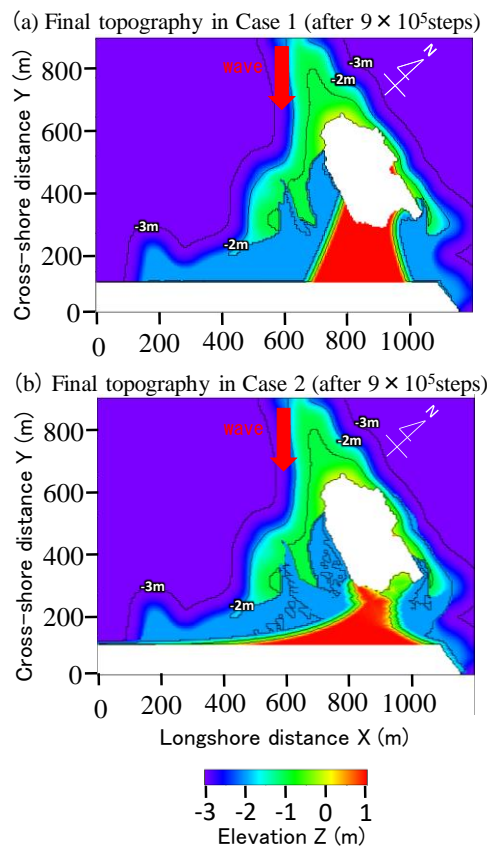


Figure 19. Comparison of final shorelines in Cases 1 and 2.

and 2 after 9×10^5 steps (2070). In Case 1, a land-tied sandbar was formed on the lee of the island, and the infinitesimal topographic variations that developed along the seawall during the development of the sandbar disappeared in the final stable topography, as shown in **Fig. 19(a)**. In addition, the shoreline behind the island intersected with the seawall at a large angle.

In Case 2, although a cusped foreland was formed, similarly to Case 1, a flatter sandbar was formed along the seawall with the shoreline smoothly connecting to the seawall. Finally, it was concluded that the sandbar behind Okinoshima Island was formed owing to waves incident from two opposing directions.

CONCLUSIONS

The shoreline changes of a land-tied sandbar formed behind Okinoshima Island located in the south part of Tateyama Bay were investigated, and the topography of the sandbar was measured using an RTK-GPS. Then, the formation of a land-tied sandbar behind the island from 1947, when no sandbar existed, to 2012 was reproduced using the BG model. In contrast, when waves were incident from offshore of the island in the direction normal to the seawall, which separates the island into halves, a cusped foreland with a small aspect ratio in the longshore direction was formed, which significantly differed from the measurement results. From these results, it was concluded that the cusped foreland behind the island was formed by waves incident from two opposing directions. Furthermore, it was found that the sand necessary for the formation of the sandbar came from the shallow seabed where sand movement owing to waves was possible after the increase in the ground level by approximately 1.6 m after the Kanto Great Earthquake in 1923.

REFERENCES

- Ashton, A., Murray, A. B., and Arnault, O. 2001. Formation of coastline features by large-scale instabilities induced by high angle waves, *Nature*, Vol. 414, 296–300.
- Chiba Prefectural Government. 1996. History of Chiba Prefecture, 639pp. (in Japanese)

- Furuya, N., Kobayashi, A., Uda, T., Noshi, Y., and Hoshigami, Y. 2014. Formation of a tombolo behind Oki Island in Tateyama Bay, Proc. JSCE (Coastal Engineering), Vol. 70, No. 2, 641–645. (in Japanese)
- Miyahara, S., Uda, T., and Serizawa, M. 2014. Prediction of formation of land-tied islands, Proc. 34th ICCE, 1–14. https://journals.tdl.org/icce/index.php/icce/article/view/7108/pdf_412
- Uda, T., 1997. Beach Erosion in Japan, Sankaido Press, Tokyo, 442pp. (in Japanese)
- Uda, T., Serizawa, M., and Miyahara, S. 2018. Morphodynamic model for predicting beach changes based on Bagnold's concept and its applications, INTEC, London, UK, 188pp. <https://www.intechopen.com/books/morphodynamic-model-for-predicting-beach-changes-based-on-bagnold-s-concept-and-its-applications>